New Journal of Physics
The open access journal for physics

Beamline, experimental stations and photon beam diagnostics for the hard x-ray free electron laser of SACLA

K Tono[1,3], T Togashi[1], Y Inubushi[2], T Sato[2], T Katayama[1], K Ogawa[2], H Ohashi[1,2], H Kimura[1,2], S Takahashi[1,2], K Takeshita[1,2], H Tomizawa[1,2], S Goto[1,2], T Ishikawa[2] and M Yabashi[2]

[1] Japan Synchrotron Radiation Research Institute, 1-1-1 Kouto, Sayo-cho, Sayo-gun, Hyogo 679-5198, Japan
[2] RIKEN SPring-8 Center, 1-1-1 Kouto, Sayo-cho, Sayo-gun, Hyogo 679-5148, Japan
E-mail: tono@spring8.or.jp

New Journal of Physics **15** (2013) 083035 (21pp)
Received 14 April 2013
Published 20 August 2013
Online at http://www.njp.org/
doi:10.1088/1367-2630/15/8/083035

Abstract. A beamline for the x-ray free electron laser (XFEL) of SPring-8 Angstrom Compact free electron LAser (SACLA) provides hard x-ray pulses in the range 4.5–19.5 keV. Its optical system in an optics hutch delivers a pink beam below 15 keV with either of two double-mirror systems or a monochromatic beam with a double-crystal monochromator. These XFEL beams are used for various types of measurement at experimental stations, e.g. x-ray diffraction, coherent diffraction imaging, x-ray spectroscopy and pump-and-probe measurement. The experimental stations consist of experimental hutches and control stations, and a femtosecond optical laser which is synchronized with XFEL pulses. Photon diagnostics have been performed for measuring radiation parameters in a shot-by-shot manner.

[3] Author to whom any correspondence should be addressed.

Content from this work may be used under the terms of the Creative Commons Attribution 3.0 licence. Any further distribution of this work must maintain attribution to the author(s) and the title of the work, journal citation and DOI.

© IOP Publishing Ltd and Deutsche Physikalische Gesellschaft

Contents

1. Introduction **2**
2. Overview of the hard x-ray beamline, BL3, of SACLA **3**
2.1. Design concept . . . 3
2.2. Layout . . . 3
2.3. Performance of BL3 . . . 4
3. Beamline optics and diagnostics **5**
3.1. Beamline optics . . . 5
3.2. Photon diagnostic system . . . 7
3.3. Advanced photon diagnostics . . . 14
4. Experimental stations **15**
5. Synchronized optical laser system **18**
6. Summary and outlook **20**
Acknowledgments **20**
References **20**

1. Introduction

Since SPring-8 Angstrom Compact free electron LAser (SACLA), an x-ray free electron laser (XFEL) facility in Japan, started user operation in March 2012, intense, coherent and ultrashort x-ray pulses have been used for experiments in various fields of science, such as structural biology, materials science, x-ray nonlinear optics and chemical physics. A coherent x-ray pulse of SACLA typically contains photons in the order of 10^{11} and has a temporal width in the order of 10 fs or smaller [1, 2]. These properties provide opportunities for investigating, e.g., structures of non-crystalline objects, nonlinear phenomena and ultrafast dynamics. The usefulness of an XFEL has been shown in recent reports of scientific applications at the Linac Coherent Light Source (LCLS) in the US [3–11].

The XFEL pulses of SACLA are generated, transported and diagnosed on a hard x-ray beamline, BL3, with undulators, beamline optics, photon diagnostic system and experimental stations. The undulators produce hard x-ray pulses in the range 4.5–19.5 keV [1]. The x-ray pulses are delivered with the beamline optics, which were designed carefully to avoid radiation damage and the degradation of the coherent wavefront.

The photon diagnostic system on BL3 measures radiation parameters such as intensity, spectrum, center-of-mass position and spatial profile. In particular, the shot-by-shot diagnostics of XFEL pulses is mandatory in the case of the photon source that is based on the principle of self-amplified spontaneous emission (SASE). The stochastic nature of the SASE mechanism induces the fluctuations of radiation parameters.

Users perform experiments at five experimental stations, each of which consists of an experimental hutch (EH) and a control station. The EHs are equipped with common-use optics and monitors. Instruments such as sample chambers and x-ray detectors can be installed in EHs for individual experiments. A femtosecond optical laser for pump-and-probe experiments has been installed in a laser booth outside the EHs.

This paper reports the design concept, detailed specification and present status of BL3. First we give an overview of BL3 in section 2. Then the design and performance of the beamline optics are shown with the basic photon-beam parameters (section 3). Section 4 gives a brief description of the experimental stations. Section 5 is devoted to the optical laser system that is synchronized with the XFEL source. Finally, we show a summary and future outlook.

2. Overview of the hard x-ray beamline, BL3, of SACLA

2.1. Design concept

In designing the beamline, we first took account of flexibility in user experiments. Basic beamline optics and photon diagnostic instruments are centralized in an optics hutch (OH) and commonly utilized for experiments at every EH. This arrangement allows us to minimize the number of fixed optical components and diagnostic instruments in the EHs. Enough space is left open in each EH to accept a variety of setups for user experiments.

Another target in our design is to facilitate the x-ray-based tuning of the XFEL machine. The optics and diagnostic system in OH are accessible from the accelerator control room for the machine tuning. For example, the double-crystal monochromator (DCM) is applied for the precise alignment of electron trajectory in the undulator section and the tuning of the undulator K parameter [1, 12]. This tuning method especially played an important role in the commissioning phase of SACLA. Intensity, position, wavelength and profile monitors are employed in the daily tuning. In addition, each beamline component is carefully designed to avoid deterioration of the wavefront of the coherent beam.

2.2. Layout

Figure 1 shows schematic drawings of BL3. Its basic constituents are undulators, electron-beam dump, x-ray transport channel in a frontend section and an OH, four EHs (EH1–EH4) in the experimental hall, and the fifth EH (EH5) in the SACLA-SPring-8 Experimental Facility.

The undulators of BL3 are placed along the center line of the undulator hall, which can accommodate five undulator lines. Two undulator lines, BL1 and BL3, have been constructed. The BL3 undulator section spans ∼110 m and contains 18 in-vacuum, variable gap undulators, each of which has a length of 5 m and a magnetic period of 18 mm. Fundamental parameters of the undulators are summarized in table 1 [1, 2].

The x-ray beamline starts after the electron-beam dump, where the electron beam is bent downward to enter a beam stop, and goes through the frontend section and the OH to the experimental stations. The OH contains the main constituents of the beamline optics, such as plane mirrors and the DCM.

The four EHs in the experimental hall are arranged in tandem. Each EH has space for two beamlines. Hutches EH1 and EH2 (EH3 and EH4) can accommodate BL4 (BL2) in addition to BL3. Since BL1 and BL5 are supposed to be soft x-ray beamlines, they will not be enclosed in EHs (see figure 1(b)). Experimental stations for BL1 and BL5 will be constructed outside the four EHs. The fifth hutch, EH5, is located ∼80 m apart from EH4. The XFEL beam and the synchrotron-radiation (SR) beam can be used simultaneously at the crossing point of BL3 and BL32XU, an undulator beamline of SPring-8.

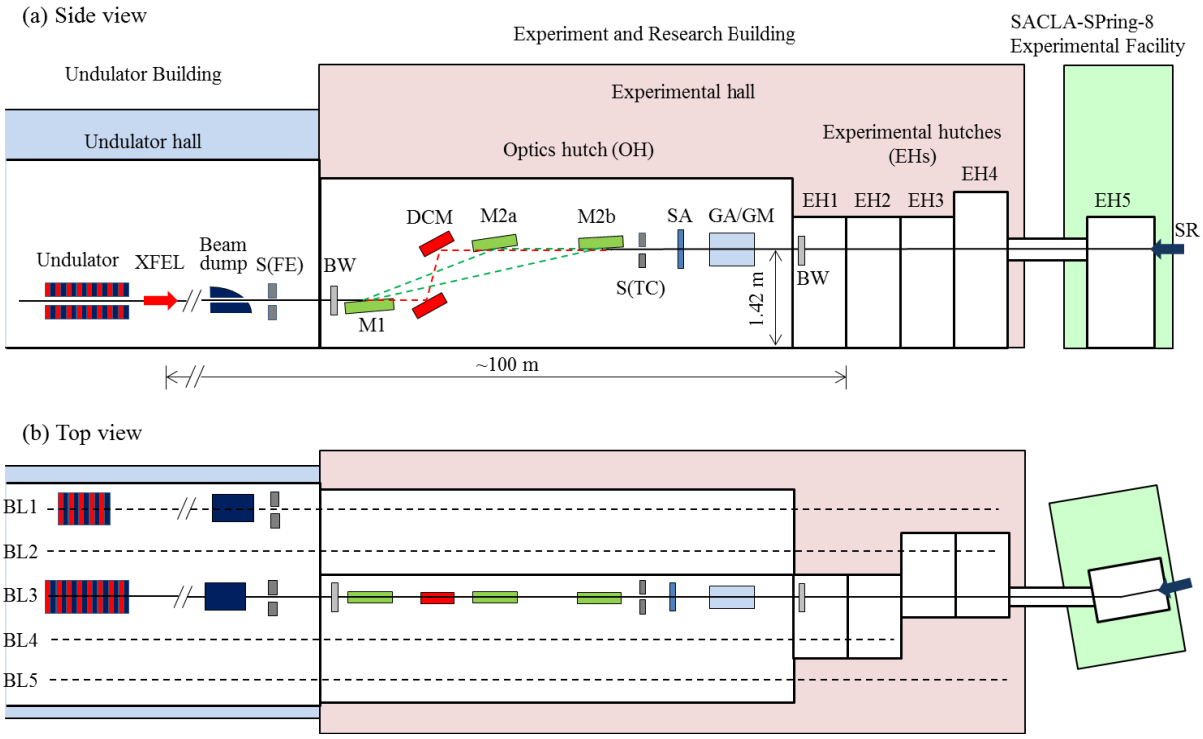

Figure 1. Schematic drawings of SACLA BL3: (a) side view and (b) top view. S(FE): slit in the frontend section; BW: Be window; M1: first total-reflection mirror (plane mirror); DCM: double crystal monochromator; M2a and M2b: second total-reflection mirrors (plane mirrors); S(TC): slit in the x-ray transport channel; SA: solid attenuator; GA/GM: gas attenuator/scattering-based gas monitor; SR: synchrotron radiation from SPring-8 BL32XU.

Table 1. Fundamental parameters of the BL3 undulator [1, 2].

Parameter	Value
Periodic length	18 mm
Periodic number	5000
Segment length	5 m
Number of segments[a]	18
Maximum deflection parameter[b]	2.3

[a] At July 2012.
[b] This value is known as a K value of an undulator. The BL3 undulator can change its K value with a variable gap length between the magnet arrays.

2.3. Performance of BL3

Since typical radiation parameters of BL3 and their design values have been reported in [1, 2], we describe them briefly in this paper. The beamline was designed to provide XFEL pulses above 20 keV as the fundamental radiation. The achieved parameters are listed in table 2.

Table 2. Typical radiation parameters of BL3 at a photon energy of 10 keV [1, 2].

Parameter	Value
Electron beam energy (GeV)	8
Repetition rate (Hz)	60 (maximum)
Undulator deflection parameter (K value)	2.1
Photon energy (keV)	10
Bandwidth	5×10^{-3}
Beam size at EH2 (mm, FWHM)	0.3
Peak power (GW)[a]	>30
Pulse energy (mJ)	0.3
Average power (W)[b]	0.02
Pulse duration (fs)	<10
Photons per pulse	2×10^{11}

[a] At July 2012.
[b] At the maximum repetition rate of 60 Hz.

At present, XFEL pulses are generated in the range 4.5–19.5 keV. The peak power at 10 keV exceeds ~30 GW with a pulse energy of ~0.3 mJ and a temporal width below ~10 fs (FWHM), which can be controlled by changing the condition of electron-bunch compression [13]. Intensity fluctuation is typically kept within 10% (one standard deviation; σ). The angular divergence (2.4 μrad in FWHM) is almost consistent with the design value (1.8 μrad). Note that the radiation parameters depend on the operation condition of the accelerator [1].

The radiation parameters shown above are the averaged values over hundreds of pulses. The results of single-shot photon diagnostics are given in section 3.3.

3. Beamline optics and diagnostics

3.1. Beamline optics

The beamline optical system basically consists of two sets of double plane mirrors and DCM [2, 14]. Figure 2 shows the configuration of the optics. The double mirrors and DCM make a vertical offset between the incident and exit beam axes for the purpose of γ-ray shielding. This offset is fixed at 20 mm without depending on photon energy. One of the mirror sets or DCM is selected to deliver an incident beam with a full or limited spectral range. The two mirror sets with different glancing angles totally reflect x-rays below cutoff energies. One set (M1 and M2a) with a 4 mrad glancing angle delivers an XFEL beam in the range below 7.5 keV, when using carbon coating. The other one (M1 and M2b) with a smaller angle of 2 mrad is applicable up to 15 keV. The plane mirrors reduce the contribution of higher order harmonics that have photon energy above the cutoff energies. The DCM with Si (111) crystals covers an energy range of 4–30 keV with a limited bandwidth in the order of 10^{-4} ($\Delta E/E$). Design parameters of the plane mirrors and the DCM are summarized in table 3.

The optical system was fabricated for the speckle-free transport of XFEL light [14]. The plane mirrors and the DCM are operated in an ultra-high vacuum condition to be free from contamination. The surfaces of the mirrors are figured and smoothed with the elastic emission

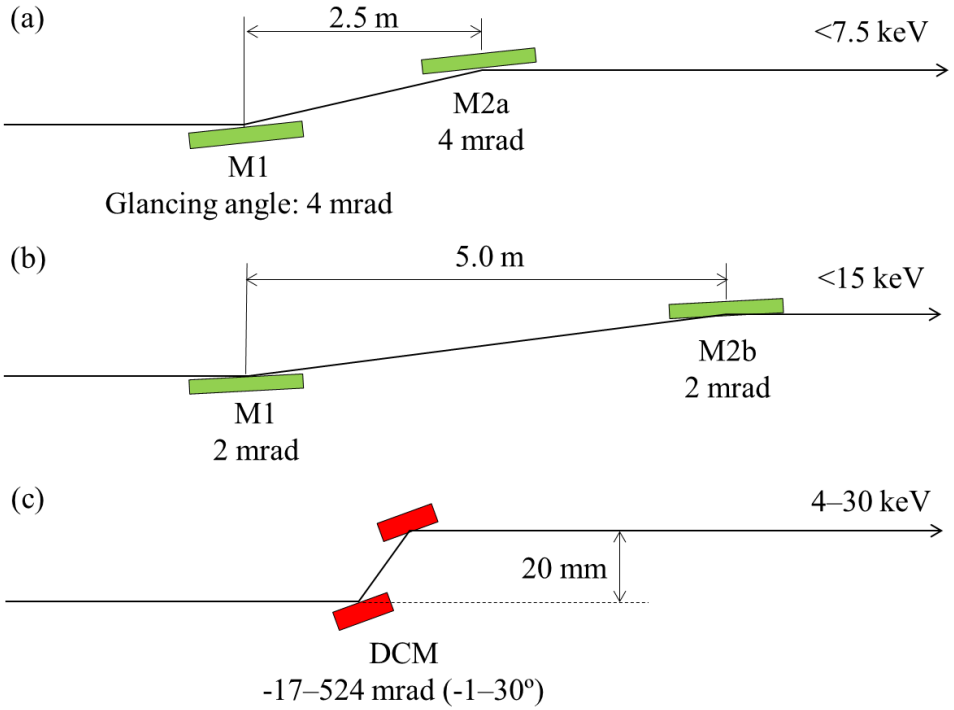

Figure 2. Three alternative configurations of the beamline optics on BL3: (a) M1 and M2a, (b) M1 and M2b and (c) DCM.

Table 3. Design parameters of the beamline optics [2, 14].

	Plane mirrors			
	M1	M2a	M2b	DCM
Distance from the exit of the undulator section (m)[a]	86.3	88.8	91.3	87.5
Glancing angle (mrad)	2–4	4	2	−17 to 524 (−1° to 30°)
Applicable range of photon energy (keV)	<15	<7.5	<15	4–30
Direction of the outgoing beam[b]	Upward	Parallel	Parallel	Parallel
Length (m)	0.4	0.4	0.4	0.09
Width (m)	0.05	0.05	0.05	0.03
Substrate	Si	Si	Si	–
Coating	–	C[c]	C[c]	–
Crystals	–	–	–	Si (111)

[a] At July 2012.
[b] With respect to the incident beam axis.
[c] A bare Si area of the surface is also available.

machining technology and ultraprecise metrologies [15]. Figure errors of 1 nm (peak-to-valley) and 0.15 nm (root-mean-square (rms)) were achieved [14].

The XFEL beam is also processed with slits and attenuators. One slit unit, which consists of a pair of L-shaped blocks, is placed in the frontend section. A 4-jaw slit is in OH, placed after the beamline optics (see figure 1). Two kinds of attenuators are employed to reduce XFEL

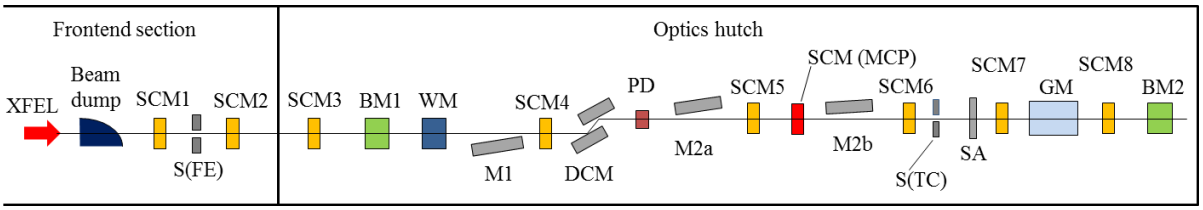

Figure 3. Photon diagnostic system on BL3. SCM1–8: screen monitor module; BM1,2: thin-foil beam monitor; WM: thin-foil wavelength monitor; GM: scattering-based gas monitor; SCM (MCP): screen monitor with a micro-channel-plate image intensifier.

intensity. A solid attenuator consists of thin silicon crystals with different thicknesses from 0.1 to 3.0 mm. It can be combined with a gas attenuator, in which Ar gas works as an absorber, for the fine tuning of intensity.

In order to separate sections of beamline at different levels of vacuum quality, vacuum-tight x-ray windows with a 0.06 mm thick Be foil are placed between the frontend section and OH, and OH and EH1. In addition, each EH is equipped with at least one Be window, which allows users to perform the experiment under ambient pressure. The Be foil transmits the XFEL beam without degrading the coherent wavefront. It is produced by physical vapor deposition, which is effective for suppressing the formation of internal voids [16]. The foil surface is polished to have an average roughness smaller than 50 nm. The speckle-free quality of the foil has been confirmed by transmission coherent-x-ray imaging at the 1 km beamline (BL29XU) of SPring-8 [16]. The Be foils are tolerant of the low average power of the XFEL beam (0.02 W at 60 Hz) even though they are not cooled. In addition, the Be windows are usually kept in a vacuum to avoid oxidation induced by x-ray irradiation. We have not observed traces of oxidation or other signs of deterioration in the film since BL3 started operation. The Be window between the frontend section and OH also works as a cutoff filter for stray light, the main source of which is broad band, coherent synchrotron radiation emitted by electrons traveling through the bending magnet in the beam dump section. The stray light can greatly affect the photon diagnostic system in OH. Since the Be windows are mounted on vacuum gate valves, they are retractable.

3.2. Photon diagnostic system

Photon diagnostic system is implemented on BL3 to provide fundamental photon-beam parameters for user experiments and the tuning of the accelerator and beamline. Figure 3 shows the monitoring system in the x-ray transport channel. Four kinds of modules are arranged for measuring spatial profile, intensity, center-of-mass position and photon energy:

1. Screen monitor (SCM) modules for spatial profile and intensity.
2. Thin-foil beam monitors (BMs) for intensity and center-of-mass position.
3. Thin-foil wavelength monitor (WM).
4. Si PIN photodiode for intensity (PD).
5. Scattering-based gas monitor (GM) for intensity.
6. SCM with an image intensifier for the x-ray-based alignment of the electron beam trajectory.

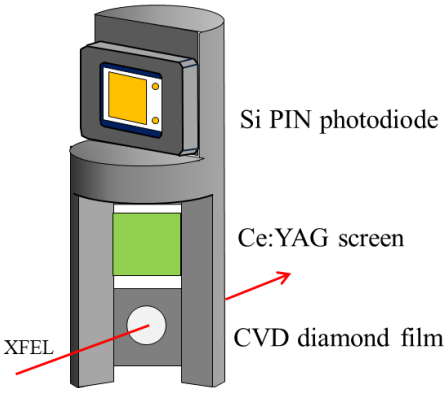

Figure 4. SCM module on BL3. It consists of a Si PIN photodiode (PD, top), a Ce:YAG screen (middle) and a boron-doped diamond screen (bottom). An incident angle for the PD (two screens) is 0° (45°).

All these monitors are able to provide photon-beam parameters in a shot-by-shot manner with the aid of the data acquisition system developed at SACLA and the SCSS test accelerator [17], which was developed as a prototype of SACLA. The same SCM modules and BMs are also implemented in EHs. The design and measurement principle of each monitor are given below.

3.2.1. Screen monitor (SCM) and photodiode for intensity in the SCM module. Figure 4 shows a schematic drawing of the SCM module which consists of two fluorescent screens and one PD. These components are usually out of the beam axis. One of them is inserted to the beam axis with a motorized linear actuator.

The two fluorescent screens work as profile monitors. One is a 0.3 mm thick plate of Ce-doped yttrium aluminum garnet (Ce:YAG) and the other is a boron-doped polycrystalline diamond film with a 0.03 mm thickness and an average surface roughness smaller than 50 nm. Fluorescent images on these screens are captured with a charge-coupled-device (CCD) camera. The Ce:YAG plate with high sensitivity is applicable to a low intensity beam in the order of 1 μJ per pulse. Because of its low x-ray transmittance, it cannot be used as an in-line monitor. On the other hand, the diamond film is able to be a nondestructive monitor. It has a high x-ray transmittance of $>97\%$ at 10 keV with speckle-free quality. Transmission coherent-x-ray imaging indicates the absence of serious voids or impurities that deteriorate the coherent wavefront of XFEL [16]. Figure 5 shows a fluorescent image on the diamond screen of SCM 3, which is placed before M1 (see figure 3). This image indicates that the beam at 10 keV has a round shape with a symmetric intensity distribution and a lateral size of $\sim$0.3 mm in FWHM.

The PD works as a highly sensitive intensity monitor [18]. It is capable of measuring an intensity in the order of 1 pJ per pulse. However, the output signal exhibits saturation behavior in the region above 0.5 μJ per pulse. Therefore, the PD is mostly applied for the XFEL beam after the DCM or the solid attenuator.

3.2.2. Beam monitor. The BM provides both the intensity and center-of-mass position of individual XFEL pulses. Its detailed design, measurement principle and performance are described in [19]. As shown in figure 6, quadrant PDs detect scattered x-rays from a 15 μm

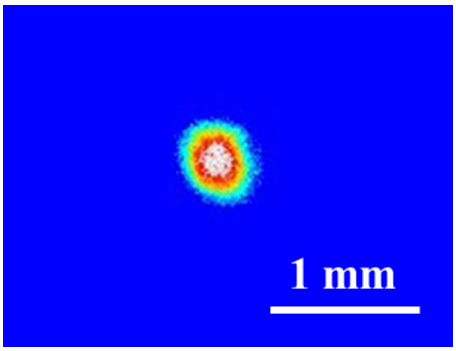

Figure 5. Spatial beam profile observed with the boron-doped diamond screen on SCM3.

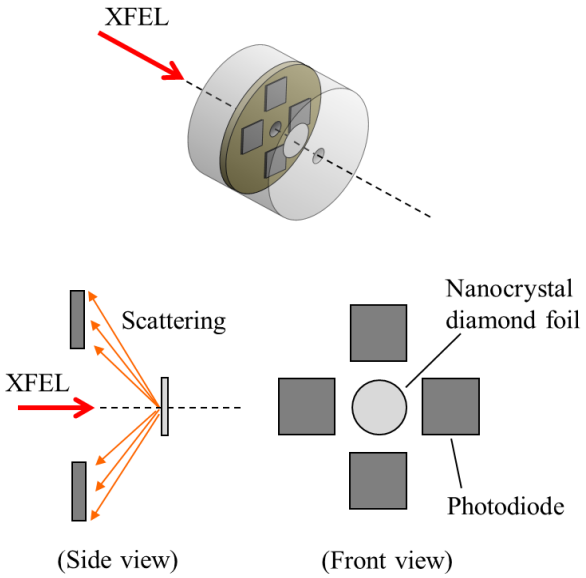

Figure 6. Schematic drawings of the structure of the BM.

thick foil which consists of randomly oriented nanocrystals of diamond. The average grain size of nanocrystals is estimated to be 34 nm by x-ray diffraction. This foil has an average surface roughness smaller than 50 nm. We confirmed the speckle-fee quality by transmission coherent-x-ray imaging [19]. The total signal of the four PDs gives intensity of the incident beam, while the difference-over-the-sum signal of upper and lower (right and left) PDs does a vertical (horizontal) displacement [20]. We have calibrated the BM with an x-ray radiometer which provides absolute pulse energies of XFEL [21]. Because of high x-ray transmittance of the 15 μm diamond foil (>98% at 10 keV), the BMs of BL3 are normally on the beam axis for in-line monitoring.

Figure 7 shows beam intensities and displacements which are measured with the BM in a shot-by-shot manner. A 10 keV beam typically has an average pulse energy of 0.33 mJ per pulse with a fluctuation of 9% (σ). The center-of-mass position fluctuates by 8 and 10 μm (σ) in the vertical and horizontal directions, respectively. The jitter and regular oscillations of the beam position mainly originate from temperature-control devices for the accelerator tubes.

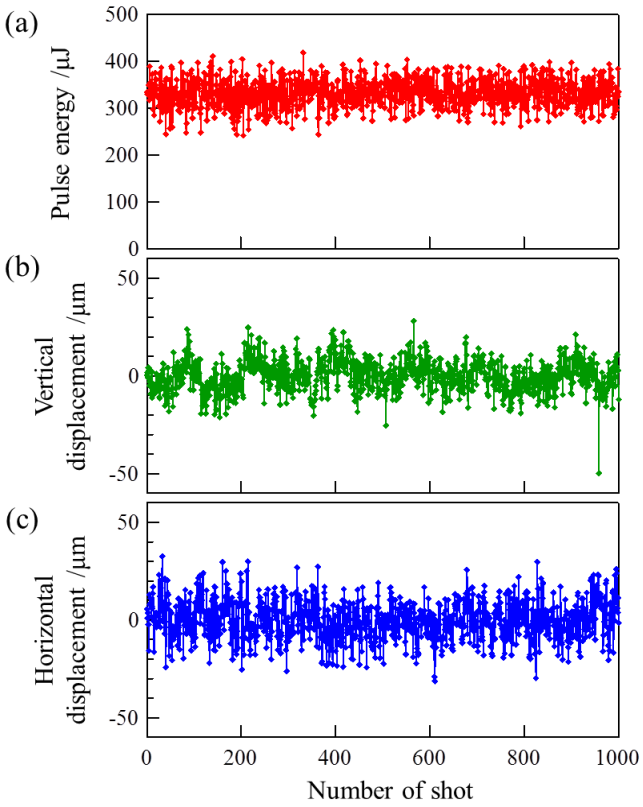

Figure 7. (a) Plot of pulse energy of the 10 keV XFEL beam as a function of the pulse number. The data were taken with BM1. (b) Vertical displacement of beam center. (c) Horizontal displacement.

The devices with pulse-width modulators induce pulsed magnetic fields that affect the electron-beam trajectory in the accelerator. The BM is usually applied to a XFEL beam in the region above 0.1 μJ per pulse. The lower-intensity beam is detected directly with a PD in an SCM module.

3.2.3. Wavelength monitor. A nanocrystalline diamond foil is also applied to wavelength monitoring. Figure 8 shows a schematic drawing of the WM, which consists of a 15 μm thick diamond foil on the center of a goniometer and a two-dimensional x-ray detector on the two-theta arm of the goniometer. The x-ray detector records shot-by-shot images of diffracted x-rays from the foil using a Si CCD sensor with eight readout ports (multi-port CCD; MPCCD). Diamond nanocrystals in the foil give a powder diffraction pattern consisting of arcs of Debye–Scherrer rings. Positions of the arcs on the MPCCD sensor provide the diffraction angle (θ in figure 8), from which the wavelength of incident light is calculated. The applicable range of the WM is currently above 6 keV, which is limited by the acceptable angle of the detector ($30^\circ < 2\theta < 60^\circ$). The 111 diffraction is used for the photon energies in 6–12 keV, 220 for 12–18 keV and 311 for >18 keV. As in the case of BMs, the WM is usually on the beam axis to be an in-line monitor.

The performance of the WM was evaluated using a monochromatized x-ray beam at BL29XU of SPring-8 [22]. Figure 9(a) shows 111 diffraction peaks of the diamond foil.

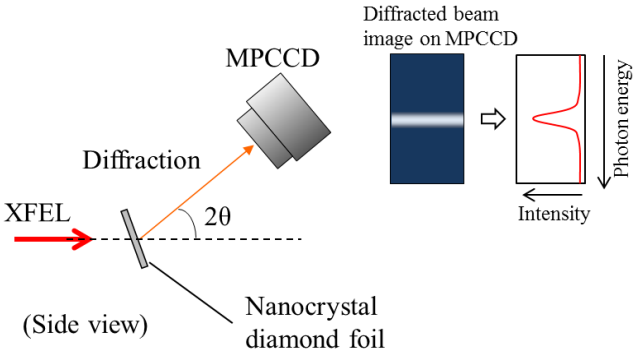

Figure 8. WM for monitoring photon energy of the XFEL beam. The nanocrystal diamond foil produces a Debye–Scherrer ring, a part of which is imaged on a MPCCD detector in a shot-by-shot manner. Photon energy is calculated from an angle of diffraction (θ).

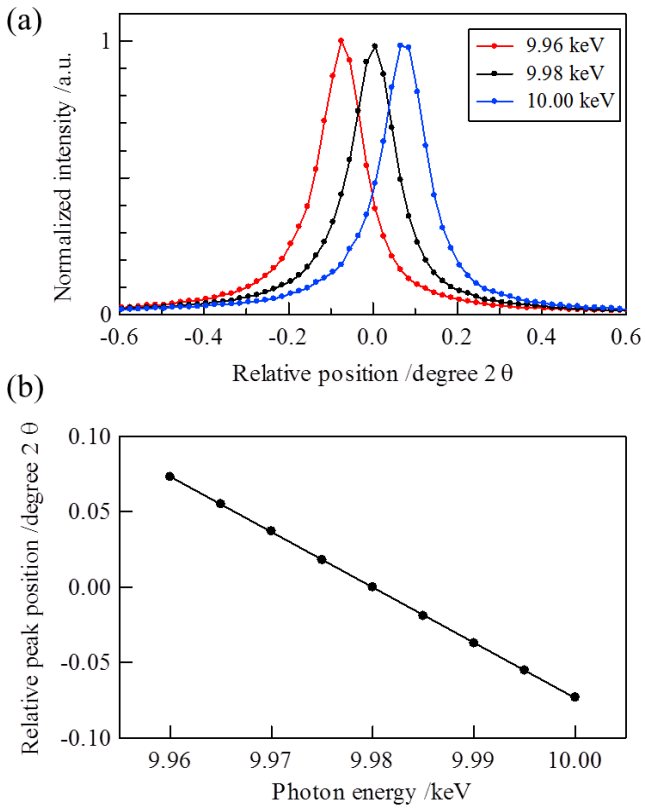

Figure 9. (a) Diamond 111 diffraction lines from the nanocrystal diamond foil. Red, black and blue curves were recorded at 9.96, 9.98 and 10.00 keV, respectively. (b) Plot of peak positions as a function of photon energy.

From these curves, the energy resolution was estimated to be ~40 eV. Although the resolution is not as high as resolving spike structures in a spectrum of SASE radiation, it is useful to monitor central photon energy (or wavelength), which is determined from the peak position of a diffraction curve (figure 9(b)). The peak position is obtained by curve fitting with an accuracy

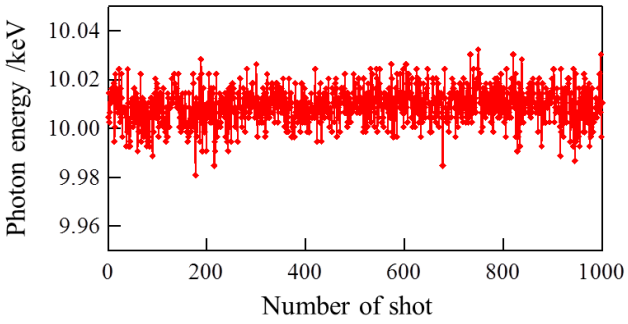

Figure 10. Photon energy data taken with the WM at individual pulses.

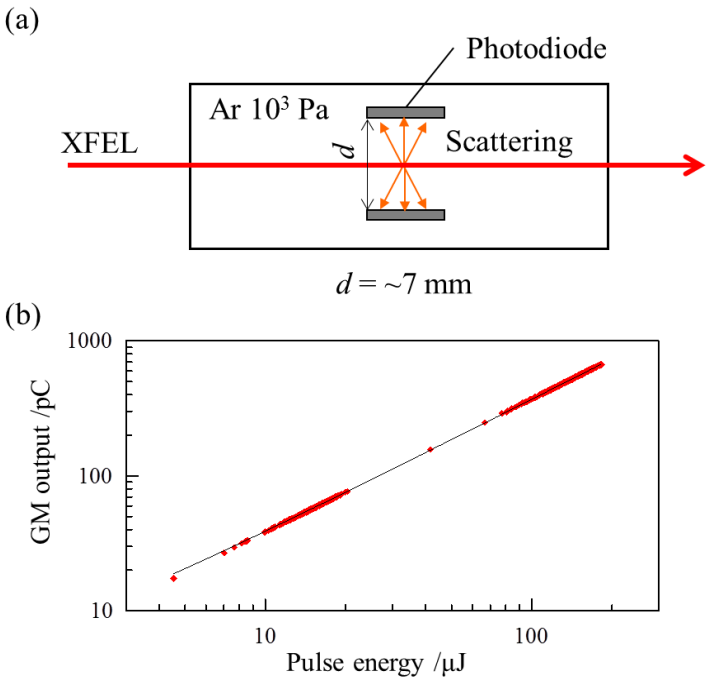

Figure 11. (a) Schematic drawing of the GM. (b) Output signals of the GM (red dots) as a function of pulse energy. Each signal is the sum of electric charges from the two PDs in the GM. The data points are well fitted with a linear function. The black line indicates the best fit curve.

of better than 5 eV. Figure 10 shows a plot of center photon energies of a 10 keV XFEL beam as a function of pulse number. A standard deviation is estimated to be only 0.07% of the average (10.009 keV), much smaller than the bandwidth (0.5%). This result indicates the stable operation of the accelerator, that is, a small jitter level of the electron-beam energy in the order of 10^2 ppm. This jitter level is smaller than the energy spread of the electron beam [1].

3.2.4. Gas monitor. Figure 11(a) schematically shows the GM. A pair of PDs in a gas chamber detects scattered x-rays from argon gas, a pressure of which is normally 1×10^3 Pa. The sum of PD signals gives the relative intensity of the incident x-ray pulse. The gas chamber is placed between two differential pumping systems which allow windowless operation of the monitor.

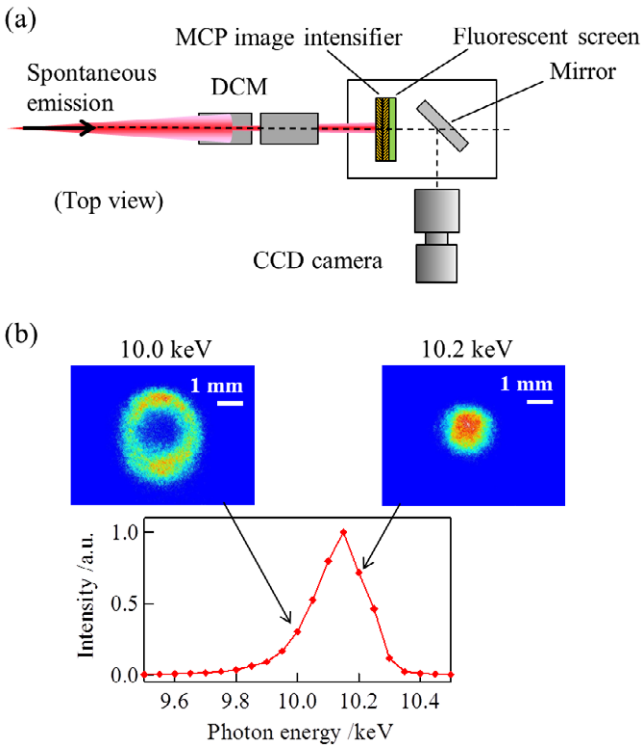

Figure 12. (a) Monitoring system of a light axis of spontaneous emission from an undulator segment. The spontaneous emission is monochromatized with the DCM to clarify the position of light axis. A SCM with an MCP image intensifier provides intensity distribution, center of which corresponds to the light-axis position. (b) Examples of a spectrum of the spontaneous emission and intensity distributions after the DCM.

An effective length of the argon-filled region is 0.5 m. Although the gas pressure is low enough for in-line monitoring, the attenuation of the XFEL beam is significant at low photon energies; for example, a transmittance is ∼60% at 4.5 keV while >90% at 8 keV. Thus, the gas chamber also works as an attenuator at low photon energies, as introduced in section 3.1. A transmittance can be controlled with the gas pressure.

The GM is suitable for high intensity pulses, which would induce saturation behavior in conventional intensity monitors such as an ionization chamber or a PD. Figure 11(b) shows a plot of signals from the GM as a function of pulse energy. The GM exhibits a linear response even in the high intensity region above 0.1 mJ per pulse.

3.2.5. SCM with an image intensifier. For the alignment of electron trajectory in the undulator section, it is necessary to monitor a light axis of spontaneous emission produced at each undulator segment [1, 12]. This light axis corresponds to the electron-beam axis in the undulator segment. Figure 12(a) schematically shows the monitoring system using a SCM with a micro-channel plate (MCP, Photonis Inc.) as an image intensifier. The DCM filters out broad off-axis radiation to clarify the position of the light axis (see figure 12(b)). Although spatial resolution of the SCM is deteriorated because of the large penetration depth of hard x-rays

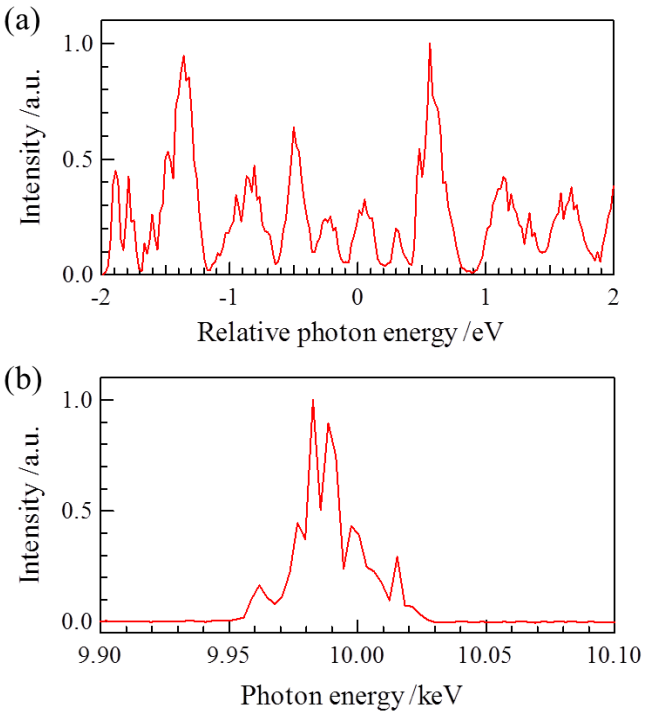

Figure 13. Single-shot spectra at 10 keV. (a) Spectrum taken by using a Si (555) analyzer crystal, which covers only a limited spectral range (4 eV). (b) Lower resolution spectrum recorded with the Si (111) reflection index ($\Delta E/E \sim 10^{-4}$), covering the full spectral range.

in the MCP, it is still sufficient for determining the center-of-mass of the monochromatized beam with an accuracy of better than 100 μm. The smeared images of spontaneous emission are mainly ascribed to the relatively low resolution of the SCM. Sharper images were obtained in higher-resolution measurement with the MPCCD detector [12]. Relative positions of light axes are determined within an angular error less than 1 μrad [12]. In the electron-trajectory alignment, deviation of the light axis is corrected by steering the electron beam with a magnet at each undulator segment. This procedure is repeated one by one for all the undulator segments.

3.3. Advanced photon diagnostics

The diagnostic systems that are described in section 3.2 are mainly used for the daily tuning of the accelerator and the beamline optics. Photon beam properties of SACLA have also been studied by using instruments dedicated for finer photon diagnostics.

3.3.1. Spectrum and pulse duration. We have developed a single-shot spectrometer which is able to resolve spike features in a spectrum of SASE radiation [13]. Figure 13(a) shows a spectrum taken with a Si (555) analyzer crystal at 10 keV. In this case, a resolution of the spectrometer is estimated to be 14 meV, high enough to observe individual peaks of longitudinal optical modes with a FWHM of ~100 meV. The spectrum covers a narrow

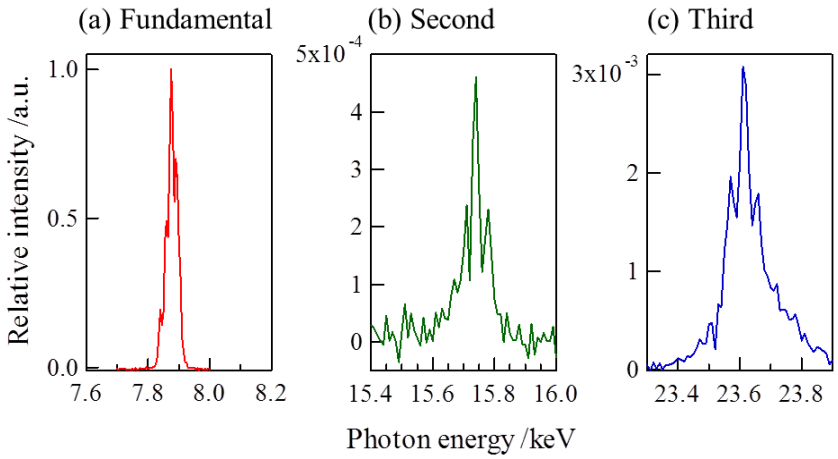

Figure 14. Spectra of (a) the fundamental radiation at 7.9 keV and its (b) second and (c) third harmonics. The spectra were measured by scanning the glancing angle of DCM.

range of 4 eV. A whole spectral range of the 10 keV radiation (typically 50 eV in FWHM) is captured in a lower-resolution spectrum, which can be simply measured with changing the reflection index to Si (111) (see figure 13(b)). Spike features are smeared in the whole-range spectrum.

The single-shot spectrometer is also applicable to the photon-beam characterization in the time domain. Widths of spikes in the higher-resolution spectrum can be related to a pulse duration, which is evaluated to be 4.5–31 fs (FWHM) on the basis of an XFEL simulation with the SIMPLEX code [13, 23].

3.3.2. Absolute intensity and the contribution of higher harmonics. A cryogenic radiometer and an x-ray GM detector were applied to measure an absolute radiant power of SACLA [21]. Results with the two independent methods agree well within a combined standard uncertainty in the order of 6–7% at 4.4, 5.8, 9.6 and 13.6 keV. The BM and the PD were calibrated with the radiometer to output reliable pulse energy data [21, 24].

The radiometer was also applied to evaluate the contribution of higher-order harmonics. The third harmonic contribution is estimated to be ∼1% of the total radiant power at 4.4 keV [21]. The contribution at different photon energies can also be measured using the DCM [1]. Figure 14 shows spectra of the fundamental, second and third harmonics at 7.9 keV. The spectra of the second (third) harmonic show a relative pulse energy of 0.05% (0.3%) in comparison with that of the fundamental radiation.

4. Experimental stations

As described in section 2, BL3 runs through the five EHs, each of which has permanently installed equipment and beam diagnostic instruments such as BMs and SCMs, which are the same as those used in OH. The latter are used for characterizing photon beam properties just in front of samples and for evaluating beamline transmission. Since these devices are compactly designed, we can keep enough space in each hutch to accept versatile experimental setups.

Table 4. Specification of the experimental stations (July 2012).

	Station 1	Station 2	Station 3	Station 4	Station 5
Distance from the undulator exit[a]	100	106	113	120	198
Hutch size					
Length (m)[b]	6	7	7	9	15
Width (m)	7	7	7	7	7.5
Height (m)	4	4	4	5	4
Optical laser		CPA[c]	CPA		
		OPA[d]			
Focusing					
Optics			KB mirrors		KB mirrors
Nominal focus size (μm, FWHM)			1		0.05
Working distance (m)			1.35		0.35
Other components	Rotary shutter	BM[e]	Guide laser	BM	BM
	Guide laser	SCM[e]	SCM	SCM	SCM
		Slit[e]		Slit	Slit
		SA[e], [f]		SA	SA

[a] From the exit of the last undulator to the entrance ports of EHs.
[b] Along the beam axis (except for Station 5; see figure 1).
[c] Output from a chirped pulse amplifier and its higher-order harmonics (800, 400, 266 nm in wavelength).
[d] Output from an optical parametric amplifier (240–1500 nm).
[e] These components are dedicated for experiments at EH3.
[f] Solid attenuator.

Most components of an experimental system, such as sample chambers, optical elements and detectors, are replaceable. Experimental systems are operated at control stations located beside the EHs. Software for the data acquisition and device control has been constructed within a framework of the message and database oriented control architecture (MADOCA) developed at SPring-8 [25].

The EHs and the control stations constitute five experimental stations, which are characterized by their geometry and permanently installed equipment as follows:

Station 1: advanced XFEL optics;

Station 2: pump and probe;

Station 3: coherent focusing;

Station 4: general purpose;

Station 5: SACLA-SPring8 mutual use.

The specifications of these stations are summarized in table 4.

Station 1: advanced XFEL optics. The first experimental station offers research opportunities mainly for advanced optics using coherent, intense and ultra-short XFEL pulses. The EH is equipped with a rotary shutter (pulse selector) and a guide laser system. The rotary shutter works as a frequency divider. A rotary disc with two channels blocks or transmits XFEL pulses to reduce a repetition rate of XFEL pulses [26]. The guide laser system provides a helium–neon laser beam as a reference for the XFEL beam axis.

Table 5. Specification of the focusing system at Station 3 [28, 29].

	Horizontal	Vertical
Focus size (μm, FWHM)	0.95	1.20
Focal length (m)	1.55	2.0
Glancing angle (mrad)	1.5	1.55
Spatial acceptance (μm)	615	632
Reflectivity	0.97	

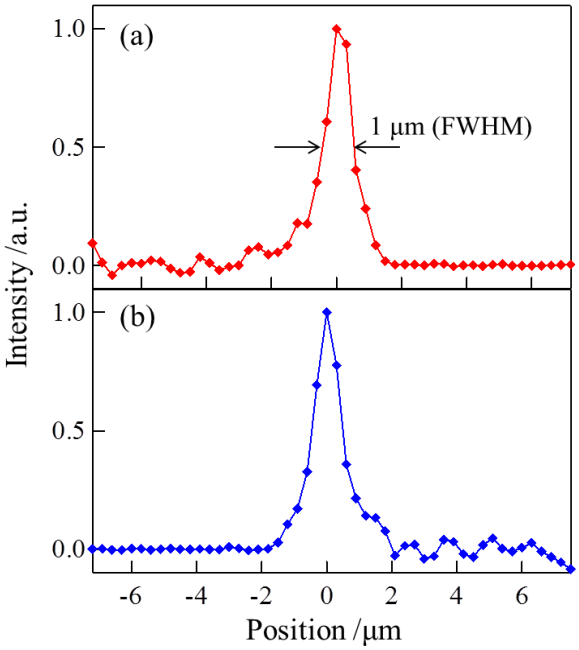

Figure 15. Focused beam profiles measured by a knife-edge scanning method. (a) Horizontal and (b) vertical profiles with 1 μm FWHMs.

Station 2: pump and probe. The second EH is equipped with fundamental optics for manipulating an optical laser beam for pump-and-probe experiments. The performance of the optical laser is described in section 5. The optical laser beam can be introduced to the sample position either on or off the axis of the XFEL beam. A compact monitor for relative arrival time of XFEL and optical laser pulses can be installed [27].

Station 3: coherent focusing. The third hutch has a focusing system consisting of a pair of concave mirrors in the Kirkpatrick–Baez geometry (KB mirrors) [28, 29]. Its specification is summarized in table 5. The KB mirrors focus the XFEL beam down to 1 μm (FWHM) at 10 keV. Figure 15 shows focused-beam profiles measured by the knife-edge scan method. The focal point is placed 485 mm away from the exit vacuum port of the focusing system. A power density at the focal point can reach 10^{18} W cm^{-2} with a pulse duration of $\sim$10 fs.

The focused XFEL beam is utilized for experiments which require high x-ray photon density; e.g. coherent diffraction imaging (CDI), x-ray nonlinear optics and femtosecond crystallography. Fundamental instruments for these experiments have been developed at SACLA. For example, sample injectors and the MPCCD detectors are available for CDI

Table 6. Specifications of Ti:sapphire CPA system.

Wavelength	800 nm
Output	5 mJ
Repetition rate	1 kHz
Pulse width	25 fs

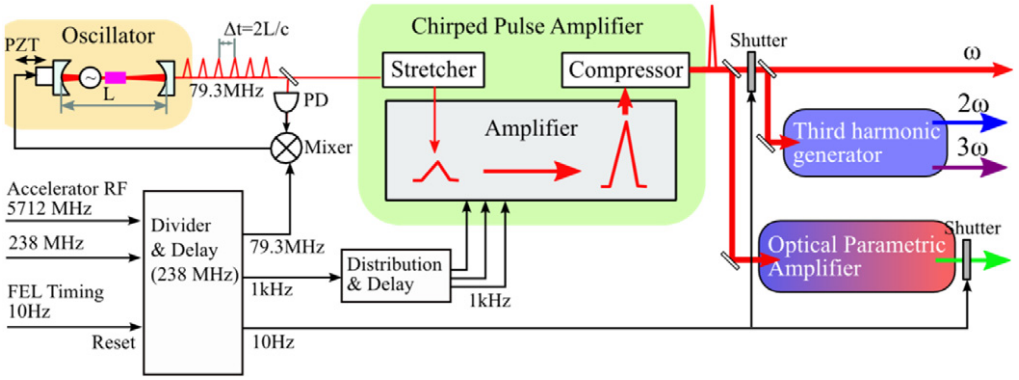

Figure 16. Schematic of the synchronized Ti:sapphire chirped-pulse-amplification system.

and crystallography. Single-shot spectrometers provide a research opportunity for novel x-ray nonlinear phenomena at high x-ray intensity [13].

Station 4: general purpose. The fourth station is suitable for a sizable apparatus because of a large capacity of EH4, which is equipped with the first KB mirrors of the two-staged focusing system for achieving an ultrasmall spot at EH5. This hutch can be used for installing a MPCCD, which records small-angle scattering produced by a sample placed at EH3. Note that the wide-angle signals can be simultaneously detected with another MPCCD, which has a central opening with a variable size below $9 \times 9\,\mathrm{mm}^2$. This MPCCD is positioned at EH3.

Station 5: SACLA-SPring8 mutual use. The fifth station is located in the SACLA-SPring-8 Experimental Facility. Both XFEL and SR beams are available at EH5, which is the terminal of SACLA BL3 and SPring-8 BL32XU. This hutch is equipped with the second KB mirrors of the two-staged focusing system, which is suitable for investigating nonlinear x-ray interactions under ultraintense x-ray fields.

5. Synchronized optical laser system

For pump-and-probe experiments between optical laser and XFEL pulses, we have constructed a Ti:sapphire (TiS) chirped pulse amplification (CPA) system (Legend Elite, Coherent Inc.) which consists of a mode locked TiS oscillator (Micra, Coherent Inc.), a regenerative amplifier and a single pass amplifier. The system generates 5 mJ output pulses at an 800 nm wavelength with a 25 fs duration (table 6). The layout of the TiS CPA system is schematically illustrated in figure 16. This laser system is operated at 1 kHz, and gated by a pulse picker to be matched with an operation frequency of SACLA (1–60 Hz). The second (SH) and third harmonics (TH) with

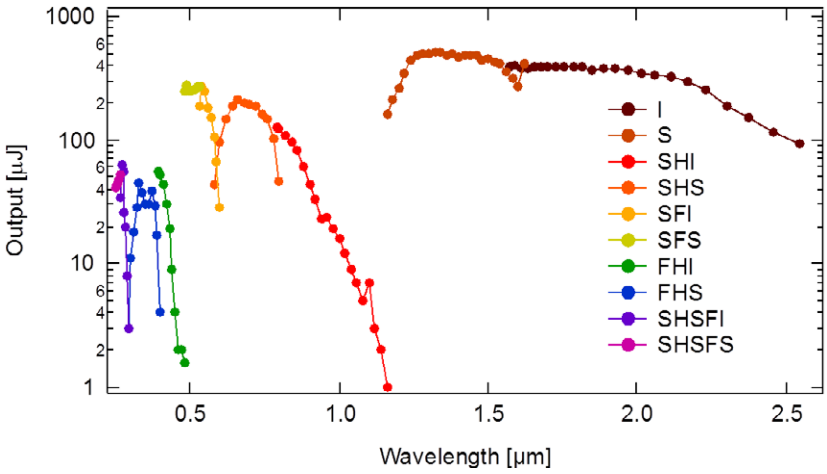

Figure 17. Output pulse energies from the optical parametric amplifier combining frequency mixer.

~0.1 mJ pulse energies are generated through BaB_2O_4 type I crystals. An optical parametric amplifier (OPA: OPerA Solo, Coherent Inc.), which is excited by partial output pulses of the TiS CPA system, generates tunable femtosecond pulses from 1.3 to 2.5 μm in wavelength. Multiple frequency mixers of nonlinear crystals convert wavelengths of the OPA output to shorter ones from the visible to ultraviolet region. Figure 17 shows output pulse energies of the OPA and multiple frequency mixers as a function of wavelength.

The TiS CPA system is seated in a temperature controlled clean hutch with a fluctuation of $\pm 0.5\,^{\circ}$C (rms). We transport the output beam to EH2 through a beam path with a 4 m length using four mirrors. Because of transportation loss, the maximum pulse energy available at EH2 is ~3 mJ. We measured fluctuations of power and pointing at EH2 to be smaller than 0.5% and 5 μrad (rms), respectively, during 12 h. In the case of the collinear setup, the optical laser beam is typically introduced to the XFEL beam axis using a turning mirror with a 1 mm center hole, through which the XFEL beam passes.

The timing of the laser pulse is synchronized to the master clock for the SACLA accelerators by feedback locking of the cavity length in the TiS oscillator (Synchrolock-AP, Coherent Inc.). The 79.3 MHz signal divided from the 238 MHz master clock is used for reference of the synchronization. We control PZT actuators, on which a cavity mirror is mounted, using the beat signal between the generating and the reference frequencies. A trigger and clock delay module (84DgR5C01, CANDOX Systems Inc.) enables us to vary the time delay between the optical laser and XFEL pulses within sub-picosecond accuracy. Frequency counters and phase shifters in this module are based on 238 and 5712 MHz RFs from the master clock. The 1 kHz trigger clock for the TiS CPA system is composed by dividing the 238 MHz clock and by being retriggered with the trigger for SACLA operation (1–60 Hz). The trigger and clock delay module can delay 79.3 MHz, 1 kHz and 10 Hz signals simultaneously with the same time step. An optical delay stage is used for precise delay control with several femtosecond accuracy. The temporal overlapping of XFEL and optical laser pulses is roughly monitored by an ultrafast metal–semiconductor–metal photodetector (G7096-03, Hamamatsu Photonics Inc.) with ~10 ps resolution.

6. Summary and outlook

The hard x-ray beamline, BL3, of SACLA offers intense, ultrashort, coherent XFEL pulses in the range 4.5–19.5 keV. The Si (111) monochromator of the beamline optics transports a narrow-band beam with a bandwidth of $\sim 10^{-4}$, while the double-plane mirrors totally reflect an incoming beam with a wider bandwidth ($\sim 5 \times 10^{-3}$ in FWHM at 10 keV). The photon diagnostic systems monitor intensity, position, profile and spectrum in a shot-by-shot manner. The beamline has five experimental stations with fundamental equipment, such as a rotary shutter, photon diagnostic systems, optical laser system and focusing systems. Both XFEL and SR beams are available simultaneously at the fifth experimental station in the SACLA-SPring-8 Experimental Facility. The optical laser system delivers femtosecond laser pulses to EH2 and EH3 for pump-and-probe experiments. Since the user operation started in March 2012, BL3 has been used for a variety of experiments, such as nonlinear x-ray optics, time-resolved x-ray diffractometry, CDI and protein crystallography.

Other beamlines will provide scientists with more opportunities for using an XFEL. A soft x-ray beamline, BL1, is currently working with one undulator module. This beamline will be upgraded by installing new undulator modules. Beamline optics and experimental stations are under construction. In addition to BL1 and BL3, SACLA can accommodate three other beamlines, one for soft x-rays (BL5) and two for hard x-rays (BL2 and BL4). A switching magnet at the end of the accelerator section divides electron bunches between beamlines [1]. The shot-by-shot switching will allow multi-beamline operation.

Acknowledgments

We thank the staff of SACLA, especially the members of the Data Acquisition Team for developing the MPCCD detectors and the control system of the beamline and experimental stations.

References

[1] Ishikawa T *et al* 2012 *Nature Photon.* **6** 540–4
[2] Goto S *et al* 2010 *XFEL/SPring-8 Beamline Technical Design Report* ver. 2.0 ed M Yabashi and T Ishikawa (Sayo: RIKEN JASRI XFEL Project Head Office, Experimental Facility Group) pp 24–35
[3] Young L *et al* 2010 *Nature* **466** 56–61
[4] Chapman H N *et al* 2011 *Nature* **470** 73–7
[5] Seibert M M *et al* 2011 *Nature* **470** 78–81
[6] Rohringer N *et al* 2012 *Nature* **481** 488–91
[7] Vinko S M *et al* 2012 *Nature* **482** 59–62
[8] Loh N D *et al* 2012 *Nature* **486** 513–7
[9] Boutet S *et al* 2012 *Science* **337** 362–4
[10] Glover T E *et al* 2012 *Nature* **488** 603–8
[11] Bernitt S *et al* 2012 *Nature* **492** 225–8
[12] Tanaka T, Goto S, Hara T, Hatsui T, Ohashi H, Togawa K, Yabashi M and Tanaka H 2012 *Phys. Rev. ST Accel. Beams* **15** 110701
[13] Inubushi Y *et al* 2012 *Phys. Rev. Lett.* **109** 144801
[14] Ohashi H *et al* 2013 *Nucl. Instrum. Methods* A **710** 139–42
[15] Mimura H *et al* 2008 *Rev. Sci. Instrum.* **79** 083104

[16] Goto S, Takahashi S, Kudo T, Yabashi M, Tamasaku K, Nishino Y and Ishikawa T 2007 *Proc. SPIE* **6705** 67050H
[17] Shintake T *et al* 2010 *Nature Photon.* **2** 555–9
[18] Kudo T *et al* 2012 *Rev. Sci. Instrum.* **83** 043108
[19] Tono K, Kudo T, Yabashi M, Tachibana T, Feng Y, Fritz D, Hastings J and Ishikawa T 2011 *Rev. Sci. Instrum.* **82** 023108
[20] Alkire R W, Rosenbaum G and Evans G 2000 *J. Synchrotron Radiat.* **7** 61–8
[21] Kato M *et al* 2012 *Appl. Phys. Lett.* **101** 023503
[22] Tamasaku K, Tanaka Y, Yabashi M, Yamazaki H, Kawamura N, Suzuki M and Ishikawa T 2001 *Nucl. Instrum. Methods* A **467–468** 686–9
[23] Tanaka T 2004 *Proc. 26th Int. FEL Conf. and 11th FEL Users Workshop* (*Trieste*) pp 435–8
[24] Tanaka T, Kato M, Kurosawa T, Morishita Y, Saito N, Yabashi M, Tono K, Kudo T, Ishikawa T and Shiraiwa S 2011 *Nucl. Instrum Methods* A **659** 528–30
[25] Tanaka R, Fukui T, Kobayashi K, Masuda T, Taketani A, Wada T and Yamashita A 1997 *Proc. of ICALEPCS'97* (*Beijing*) pp 1–4
[26] Kudo T, Hirono T, Nagasono M and Yabashi M 2009 *Rev. Sci. Instrum.* **80** 093301
[27] Sato T, Togashi T, Tono K, Inubushi Y, Tomizawa H, Tanaka Y, Adachi S, Nakamura K, Kodama R and Yabashi M 2013 *J. Phys.: Conf. Ser.* **425** 092009
[28] Yumoto H *et al* 2013 *Nature Photon.* **7** 43–7
[29] Yumoto H *et al* 2013 *J. Phys.: Conf. Ser.* **425** 052022